Effect of etching on the composition and structure of anodic spark deposition films on titanium

E. Marin [a], M.V. Diamanti [b,c,*], M. Boffelli [a], M. Sendoh [a], MP. Pedeferri [b,c], A. Mazinani [b], M. Moscatelli [b], B. Del Curto [b,c], W. Zhu [d], G. Pezzotti [a], R. Chiesa [b,c]

[a] Ceramic Physics Laboratory, Kyoto Institute of Technology, Kyoto, Japan
[b] Department of Chemistry, Materials and Chemical Engineering "G. Natta", Politecnico di Milano, Milan, Italy
[c] INSTM - National Interuniversity Consortium of Materials Science and Technology, Florence, Italy
[d] Department of Medical Engineering for Treatment of Bone and Joint Disorders, Osaka University, Osaka, Japan

Anodic spark deposition is particularly spread as coating treatment of titanium in biomedical applications, as it allows to improve both durability and biocompatibility of titanium and its alloys. This work proposes an analysis of different surface treatments on titanium, where surface etching in HF prior to anodizing and final alkali etching of the anodic oxide are chosen as possible methods to alter surface roughness, crystal structure and chemical composition. Anodizing was performed at two different voltages to produce different morphologies and crystal phases. Larger and more regular porosity was obtained at higher voltages, together with the formation of sodium titanates. While the HF pre-treatment only affected surface roughness but not surface chemistry, the NaOH post treatment promoted the formation of Na_2TiO_3 especially on high voltage formed oxides. This was identified as the cause for a larger presence of radical species, which modify surface bioactivity and is responsible for a bacterio-static effect of the treatments reported in previous biological studies.

Keywords:
TiO2
Anatase
Anodic spark deposition
Raman spectroscopy
Na2TiO3

1. Introduction

Titanium anodizing is a consolidated technology that is used to produce the formation on the metal of an oxide film, always based on titanium dioxide (TiO_2) formation but with different thickness, crystal structure, morphology and composition depending on process parameters [1,2]. This treatment is particularly spread in biomedical applications, where the favourable combination of mechanical properties, durability and biocompatibility of titanium and its alloys make them particularly suitable for dental and orthopaedic implants, as well as for ostheosynthesis devices [3,4]. In such field, first applications of titanium alloys – mostly as hip joints and dental implants – date back to 1940s, while the development of ad hoc titanium anodizing treatments started in late 1970s to further improve biocompatibility, aimed at optimizing surface topography, enhancing corrosion resistance, and manipulating oxide composition [5,6]. Anodic spark deposition (ASD, also called plasma electrolytic oxidation, PEO, or microarc oxidation, MAO) is currently the most frequently adopted anodizing treatment for titanium as biomaterial [7]: it causes the growth of a thick, crystalline ceramic oxide, with porous microstructure and composition altered by the incorporation of ions from the electrolyte. The coatings can have high micro-hardness, excellent adhesion and strength, and improved wear resistance, which is one of the major drawbacks of titanium implants [5,7–9].

More specifically, surface modifications of titanium bone implants address specific requirements that are vital to foster positive interactions between the implant and surrounding tissues, maintaining the characteristics of a bioinert surface through a reduction of ionic release phenomena, or turning it into a bioactive one, thus favouring osseointegration, bone ingrowth, cell proliferation and differentiation. Another interesting task of a bioactive surface would be the obtaining of an antimicrobial action. This may be achieved by two main routes, i.e., either by coating/loading TiO_2 surfaces with antibiotics, peptides, or other suitable drugs [10], or by introducing other metal species with bacteriostatic capabilities in form of ions, nanoparticles, or nanocomposite with TiO_2 [11,12].

Yet, titanium dioxide may itself show antimicrobial activity, as emphasized in several reviews [13–15]. This can be associated with the well-known photocatalytic activity of titanium dioxide, which promotes redox reactions between light-activated TiO_2 and water with consequent generation of hydroxyl radicals and superoxide ions: these in turn react with compounds present in the surrounding environment, in this case with bacteria or other microorganisms, causing their

* Corresponding author at: Department of Chemistry, Materials and Chemical Engineering "G. Natta", Politecnico di Milano, Via Mancinelli 7, 20131 Milan, Italy.
E-mail address: mariavittoria.diamanti@polimi.it (M.V. Diamanti).

Published Journal Article available at: http://dx.doi.org/10.1016/j.matdes.2016.06.088

degradation and/or inactivation [16–18]. Reactive oxygen species are always indicated as responsible for the antimicrobial activity observed.

Although TiO_2 needs light irradiation, and specifically UV light, to induce the formation of such species, an antibacterial effect was noticed in a previous study on anodic TiO_2 layers prepared by ASD and further modified by alkali etching [19]. This activity towards a multidrug resistant bacterium was observed to be close to the behaviour of similar anodic layers modified with the addition of silver [11]. One mechanism was envisioned as responsible for this unexpected antibacterial activity, that is, the formation of reactive oxygen species due to non-stoichiometry of the oxide film, and particularly to a large content of Ti^{3+} species as a result of oxygen vacancies: this, together with other features related to TiO_2 nanoparticles rather than to anodic surfaces, was already proved to be a possible source of antimicrobial effects [20,21].

To evaluate this hypothesis, here we present a large experimental campaign aimed at investigating the morphological, chemical and struc-tural properties of anodic TiO_2 films obtained by ASD in silicates, and the effect of alkali etching on their properties. To meet this aim, the samples were fully characterized using Raman spectroscopy. From the Raman spectrum of TiO_2 many different information can be obtained: titanium oxide phase fraction [22,23], crystallinity, crystallite size [24] and resid-ual stresses [25] down to a minimum coating thickness of about 100 to 250 nm, depending on the substrate chemistry [26]. Crystallographic al-terations caused by small amounts of dopants into the TiO_2 structure can also be easily discriminated by the appearance of their associated Raman bands [27], thus making Raman spectroscopy adequate for the characterization of functionalized titanium oxide layers [28–30]. The presence of a characteristic Raman spectrum associated with sodium ti-tanate and clearly discernible from the anatase and rutile spectra [31] was used in order to evaluate the influence of the anodizing bath composition and of the NaOH post-treatment on the final chemistry of the titanium oxide surface, in particular taking into account that bioactivity of sodium titanate, which plays an important role on the osseointegration rate [32,33].

2. Experimental

2.1. Sample preparation

Anodizing treatments were performed on 12 mm diameter 0.5 mm thick titanium discs. Ten discs were punched with a mechanical cutter from a commercially pure grade 2 medical grade (ISO 5832-2) titanium sheet. All punched discs were cleaned and degreased by ultrasonic rinsing in acetone for 10 min, then by ultrasonic rinsing in Millipore water for other 10 min. The ten discs were finally dried in a thermostat oven at 37 °C for 1 h.

After cleaning, five discs were etched (E) for 120 s in a water solution containing 5% (v/v) of hydrofluoric acid and 20% (v/v) of nitric acid.

An Anodic Spark Deposition (ASD) treatment was performed on eight discs as described elsewhere [34]. Briefly, the considered ASD treatments were performed in a water solution kept stirred and maintained at 0 °C (±1 °C). The considered solution contained silicon, calcium, phosphorous and sodium. In particular, the solution composition was: 0.03 M of $Na_2SiO_3{*}2H_2O$ + 0.1 M of β-glycero-phosphate ($C_3H_7Na_2O_6P{*}5H_2O$) + 0.3 M of calcium glycero-phosphate ($C_3H_7O_6PCa$) + 0.036 M of NaOH. All reactants were purchased by Sigma-Aldrich. During the treatment, the titanium disc was connected as anode to a DC power supply (National Instruments), while a titanium mash was used as cathode. The ASD treatment was performed in galvanostatic conditions, imposing 10 mA/cm^2 up to two different final voltages: 175 V for four discs and 295 V for other four discs. Final voltage for ASD 175 V was reached in 1′18″ ± 4″ treatment time, while for ASD 295V samples the electrochemical treatment duration was 8′41″ ± 18″, for etched and not etched samples.

A final alkali etching in a 5 M NaOH water solution for 2 h at 60 °C was performed on four different discs.

Fig. 1 summarizes the treatments involved in the preparation of each of the 10 samples. For brevity, samples etched before ASD will be referred as “E” and not-etched as “NE”. “175 V” and “295 V” will indicate the final voltage reached by the ASD treatments. The wording “+NaOH” will indicate if the sample was finally alkali etched.

2.2. Characterization techniques

The morphological characterization and roughness analysis of the samples surfaces was carried out using a confocal laser microscope (Keyence, VK-x200 series, Osaka, Japan) with a 408 nm wavelength laser source. The instrument high depth field and good spatial resolutions granted reliable results in the range between 100× to 1500× magnifications. For statistical purposes, at each magnification 9 maps were acquired on each sample at randomized locations. Roughness (Ra) was then measured and averaged between different acquisitions.

A Field Emission Gun Scanning Electron Microscope (FEG-SEM, SE-4300, Hitachi Co., Tokyo, Japan) was used to observe the surface morphology at higher magnifications. The instrument is equipped with an Electron Dispersive X-ray Diffraction (EDS) probe and a Cathodoluminescence (CL) device. All images were collected at

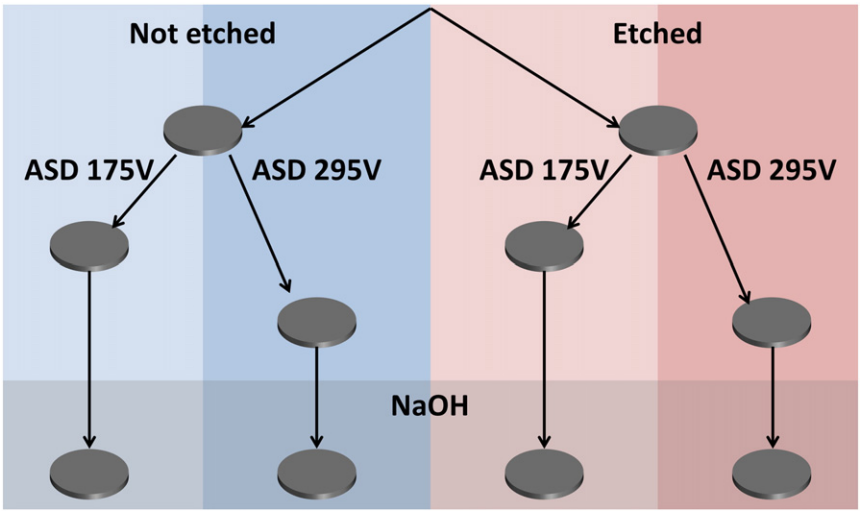

Fig. 1. Schematic representation of surface treatments on titanium.

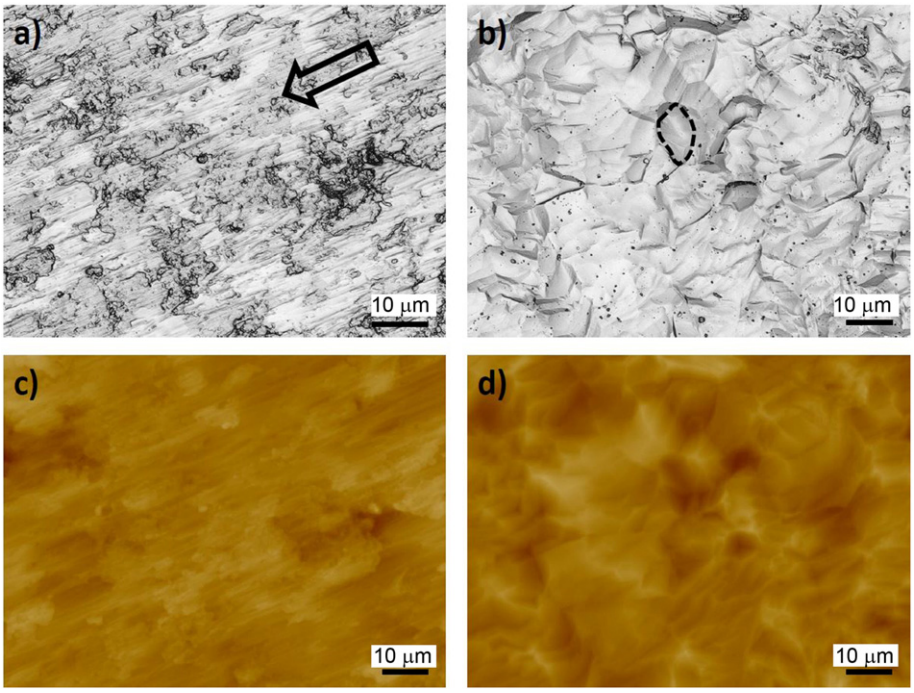

Fig. 2. Surface morphology (a, b) and topographical maps (c, d) of titanium before (left) and after (right) etching, as observed by confocal laser microscopy.

low acceleration voltage (5 kV) at magnifications comprised between 2k× and 70k×.

All the Raman spectroscopic experiments described in this paper were carried out in a backscattering configuration using a triple monochromator (T-64000, Horiba/Jobin-Yvon, Kyoto – Japan) equipped with liquid nitrogen-cooled charge coupled device (CCD), a confocal pinhole, and (cross or parallel) polarization filters. In the present experiments, the excitation source used was a 532 nm Nd:YVO_4 diode-pumped solid-state laser (SOC JUNO, Showa Optronics Co. Ltd., Tokyo, Japan) operating at the power of 200 mW. A neon lamp and a silicon substrate (111) were used for the internal calibration of the spectrometer. An objective lens with a numerical aperture of 0.5 was used both to focus the laser beam on the sample surface and to collect the scattered Raman light. For each sample, 9 maps composed by 11 × 11 punctual Raman acquisitions were processed. Each acquisition was performed on an interval of 10 s for 2 repetitions, in the range between 0 and 800 cm^{-1}. The average Raman profile was then considered as representative for the overall sample surface.

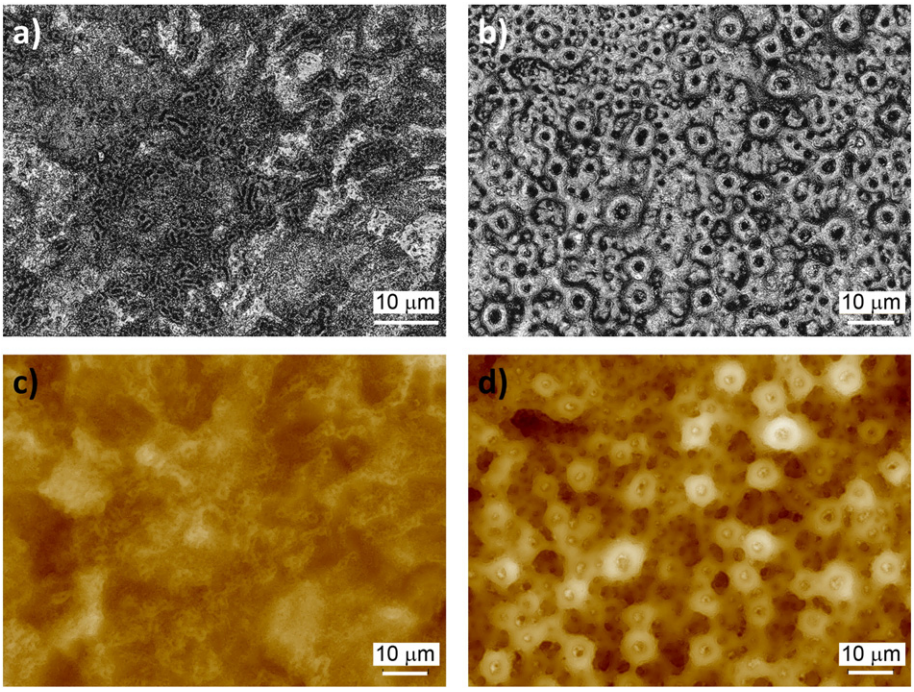

Fig. 3. Surface morphology (a, b) and topographical maps (c, d) of titanium anodized at 175 V (left) or at 295 V (right), as observed by confocal laser microscopy.

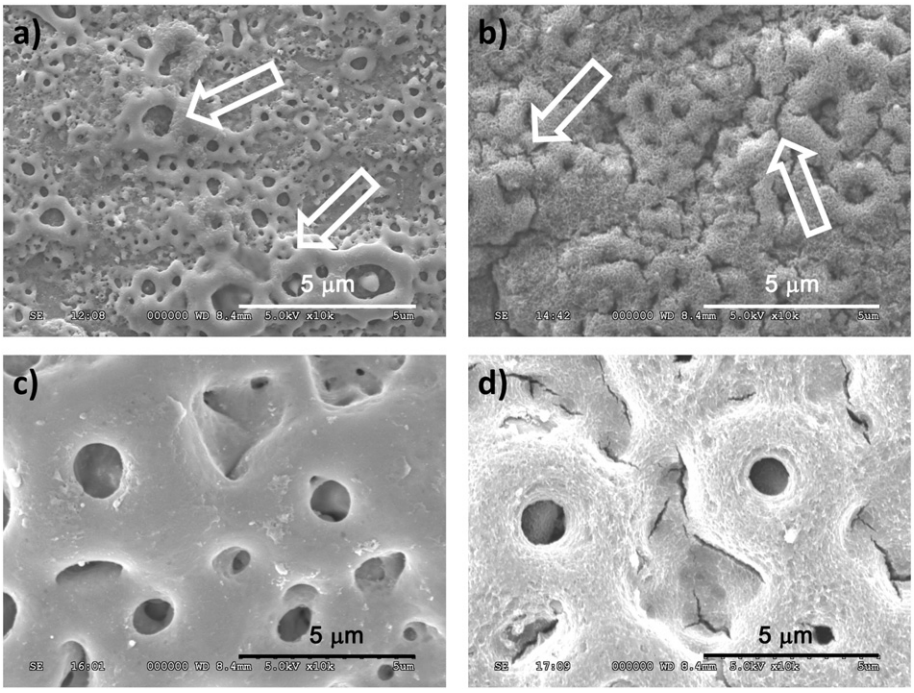

Fig. 4. SEM images obtained on the different etched samples at 20k × magnifications: a) sample E 175, b) sample E 175 OH, c) sample E 295, d) sample E 295 OH.

3. Results and discussion

The surface morphology of titanium before (a, c) and after (b, d) etching with a HF solution, as acquired by confocal laser microscopy, is presented in Fig. 2. The noticeable oriented scratches caused by the machining of the sample can be easily spotted on Fig. 2a (the arrow mark indicates the direction of the machining), but they are completely removed by etching, as evident from Fig. 2b, where some grain bound-aries have also been enlightened, showing an equiaxial microstructure (blue marks for one example) with an average grain diameter in the range of 10–20 µm. As it can be observed by the topographical maps of Fig. 2c and Fig. 2d, etching clearly increases the surface roughness of the pristine titanium substrate.

The specific effect of each ASD treatment on surface morphology is clearly visible in the laser microscope images of Fig. 3. For the E 175 V treatment (Fig. 3a), the surface appears to be covered by a discontinu-ous, porous oxide layer with pore diameters up to two microns. The pores are of irregular, elongated shape and they are surrounded by a rel-atively thin border of protruding titanium oxide. In the discontinuity re-gions noncovered by the distribution of pores, the surface appears to be pocked and rough. No morphological differences could be clearly spot-ted in comparison with the not-etched substrate and with the NaOH post-treatment using confocal laser microscopy.

A completely different morphology appears on the samples anod-ized at the higher potential, E 295 V (Fig. 3b). Pore distribution is more homogeneous and the average diameter is bigger, reaching almost 5 µm. The pores are surrounded by a thicker border of protruding titani-um oxide, forming a dispersion of crater-like structures. As in the previ-ous case, no clear morphological differences between etched, not-etched and NaOH post-treated samples were observed by laser microscopy.

More information can be derived from surface topographic images. Fig. 3c shows the topographic morphology of the E 175 V sample. It can be observed that the underlying topography is similar to the etched surface of Fig. 2d, meaning that the treatment does not drastically mod-ify the roughness of the titanium substrate on which it is applied. Changing the ASD voltage clearly modifies the surface morphologies of the samples, as can be observed from a comparison between Fig. 3c and the E 295 V sample surface of Fig. 3d. The increase in roughness is evident and the features of the substrate are completely covered by the deposited oxide layer.

Fig. 4 summarizes the SEM images obtained on the different etched samples at 20k× magnifications. In Fig. 4a, a dispersion of porosities with different diameter, from few hundred nanometers to about 3 µm, is visible on the surface of the E 175 sample. The effect of the treatment

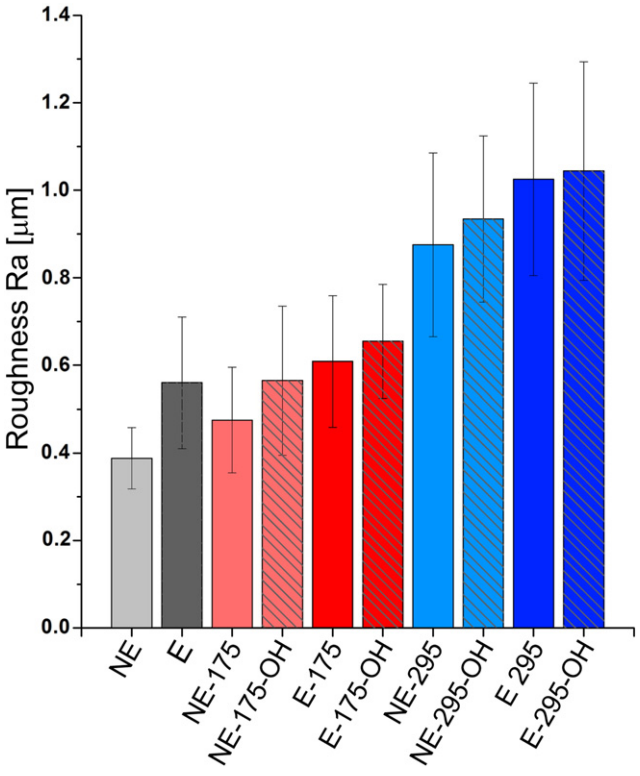

Fig. 5. Roughness of samples subjected to different surface treatments.

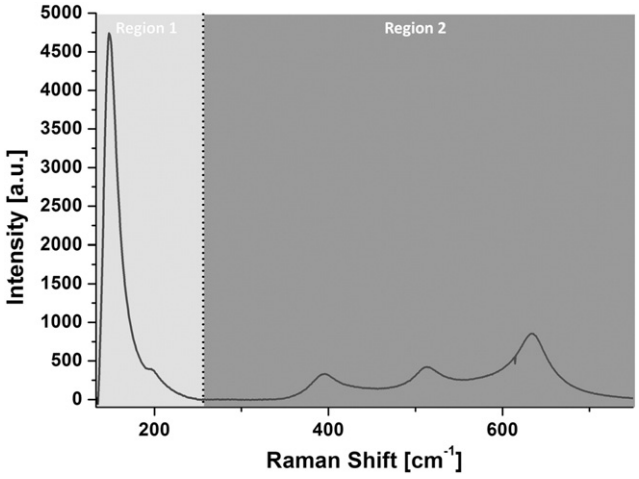

Fig. 6. Raman spectrum of sample anodized at 175 V, with no etching treatment.

is not uniform and the ASD oxide layer is thicker around the larger porosities, forming a crater with a smooth external surface (arrow marks). The application of a NaOH post-treatment (Fig. 4b) drastically modifies the sample, generating a wrinkled surface on which a net of cracks can be clearly spotted (arrow marks). From a comparison with Fig. 4a, it seems that not only the craters of the ASD oxide layer but also the smooth and compact base oxide is etched by the post-treatment. Fig. 4c shows the surface of the E 295 sample. The treatment is more uniform when compared to Fig. 4a, with larger porosities and thicker oxide craters with a smooth surface. When the NaOH post-treatment is applied, once again the surface becomes rough and a net of cracks is generated in the region between different craters. No sensitive difference was observed between etched and non-etched substrate using SEM.

Further confirmations on the morphological alteration effect of the different surface treatments can be deducted from the roughness graph of Fig. 5, which reports the average values of R_a – measurement variability is also reported, and is equivalent on all samples. As previous-ly stated, HF etching has a clear effect in enhancing surface roughness of titanium by about 40%. This effect is superior to the standalone ASD treatment at 175 V - which causes an increase of about 15% - but slightly lower than the combination of etching and ASD treatment, which together generate an increase of about 50%, meaning that the dominant contribution to the roughness of the 175 V samples is caused by etching. A subsequent treatment in NaOH brings surface roughness of the non-etched 175 V sample to an overall increase of about 40%, close to values

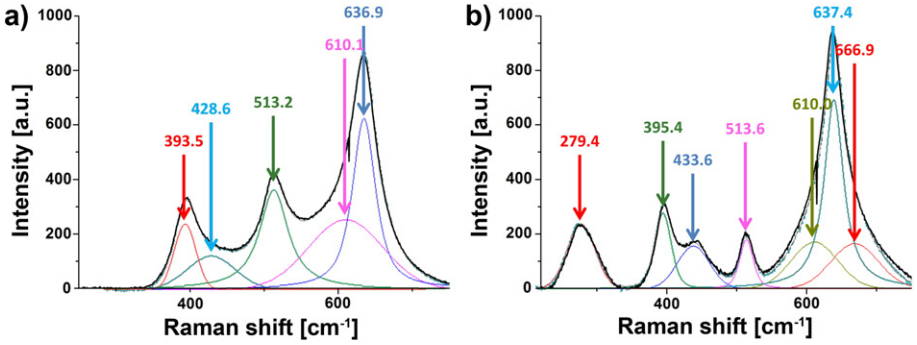

Fig. 7. Different Raman spectra deconvolutions of region II: a) NE 175 V spectrum, b) NE 295 V + OH spectrum.

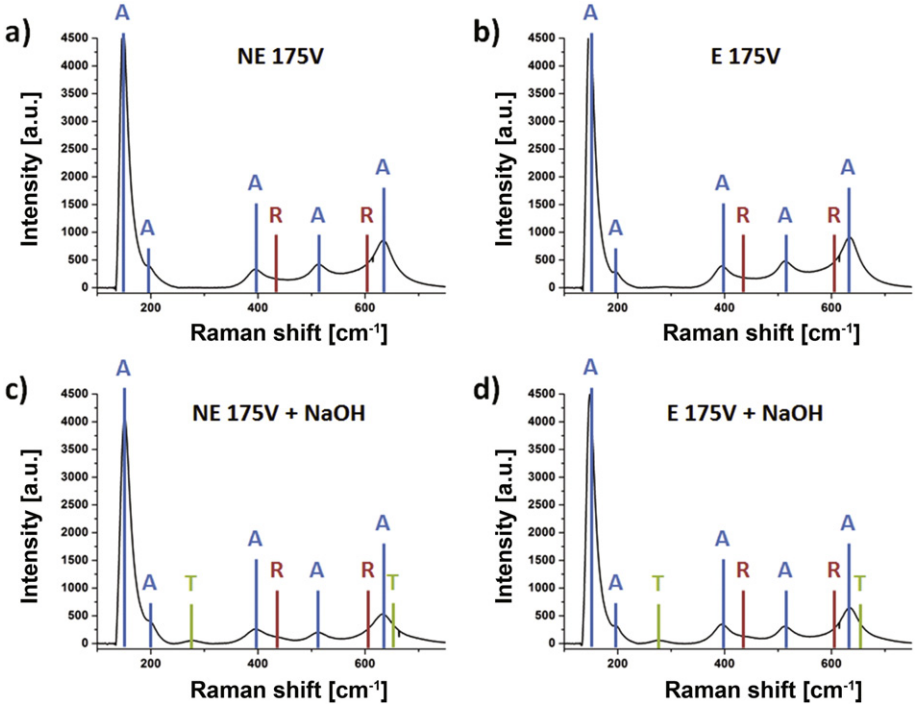

Fig. 8. Raman spectra obtained on 175V treated samples: a) NE 175 V, b) E 175 V, c) NE 175 V + OH, d) E 175 V + OH.

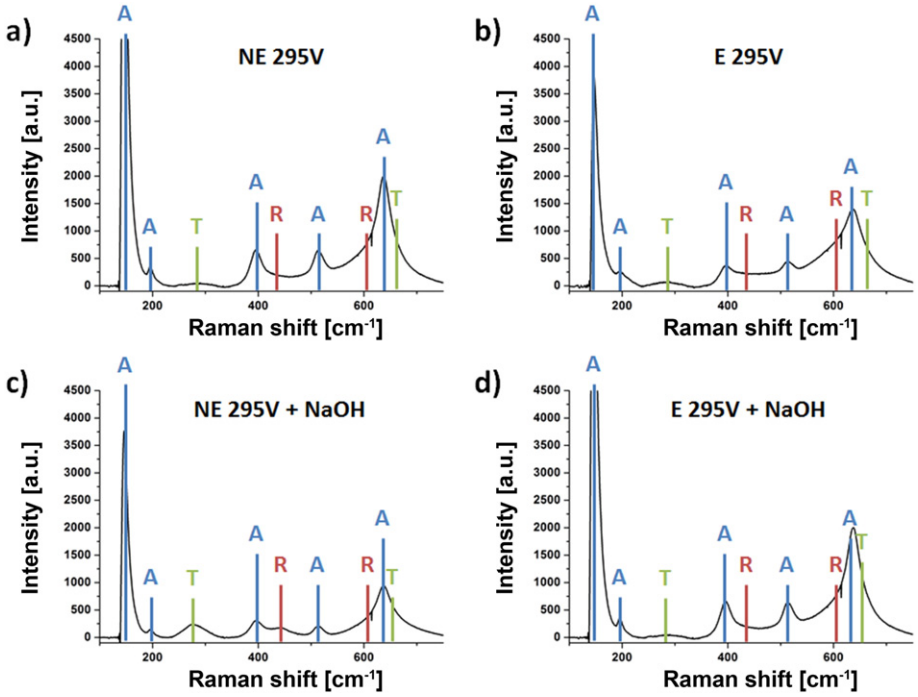

Fig. 9. Raman spectra obtained on 295V treated samples: a) NE 295 V, b) E 295 V, c) NE 295 V + OH, d) E 295 V + OH.

obtained for the etched substrate, and that of the etched 175 V sample to even higher values, with an overall increase of about 55%. At 295 V, even in the case of not-etched substrates, roughness values are more than two times higher (increase of 130%) with respect to pristine titani-um, and they are further augmented by a subsequent NaOH treatment, for a total increase in roughness of about 140%. The combination of etch-ing and anodizing at 295 V gives the highest surface roughness, reaching a total increase of about 160%, but the subsequent NaOH treatment shows only a limited effect, increasing the roughness to about 165% of that of pristine titanium.

Fig. 6 shows a representative Raman spectrum obtained on the NE 175 V sample. The spectrum has been divided in two regions, region I up to 300 cm^{-1} and region II from 300 cm^{-1} to 750 cm^{-1}. The first region features two peaks that are commonly associated with the anatase phase of TiO_2, one more intense at about 146 cm^{-1} and a smaller one at about 195 cm^{-1}. Region II features three visible peaks with an intensity comparable with the 195 cm^{-1} peak of region I. Due to the high relative intensity of the 146 cm^{-1} and the associated difficulties in peak deconvolution in that region, analyses were focused on region II.

Fig. 7 shows two different Raman spectra deconvolutions of region II, as obtained for NE 175 V (Fig. 7a) and NE 295 V + NaOH (Fig. 7b) samples. It can be observed that the best fitting of the spectra for Fig. 7ais obtained using not three but five different Raman bands due to the asymmetric shape of the first and last peaks of the spectra. The five peaks are at about 394, 429, 513, 610 and 637 cm^{-1}. Of those, three peaks are associated with the anatase phase, namely 394, 513 and 637 cm^{-1}, while two peaks are associated with the rutile phase, namely 429 and 610 cm^{-1}. Due to its shape, completely covered by the stronger 637 cm^{-1} peak, the position of the 610 cm^{-1} had to be set in the deconvolution considering previous literature data on rutile [35,36].

For the NE 295 V + NaOH, the best fitting was obtained taking into account the previous five Raman bands plus additional two, one of which at about 279 cm^{-1}, the other (667 cm^{-1}) hidden under the stronger peak at 637 cm^{-1}, broadening it. The complete peak list for this sample is then 279, 395, 434, 514, 610, 637 and 667 cm^{-1}, which are associated to the previously observed anatase and rutile phases plus, at least, a third phase. Literature data [37–40] support our hypothesis of the third phase being formed by a mixture of sodium titanates and sodium hydrogen titanates with different stoichiometry, with a higher fraction of Na_2TiO_3, which in literature is associated in particular with the 279 cm^{-1} peak. Other more complex $Na_xTi_yO_{xy+1}$ sodium tita-nates, such as $Na_2Ti_6O_{13}$ [41] and $Na_2Ti_3O_7$ [42], feature an additional strong peak at 671 cm^{-1}. The formation of wrinkles on the surface of TiO_2 also supports the formation of titanates, which were previously shown to create a three-dimensional network of fibers and wrinkles on a titanium alloy immersed in NaOH [39,43].

Fig. 8 shows the Raman spectra obtained on all the 175 V treated samples. The position of the different bands is marked with the letter "A" for the anatase phase, "R" for the rutile phase and "T" for the sodium titanate phase. It can be observed that samples anodized at low voltage and not subjected to final alkali etching (Fig. 8a, b) do not feature the "T" associated bands, therefore no titanates were revealed, while the NaOH treatment (Fig. 8c, d) produced on both etched and non etched samples the appearance of "T" bands, even if with low relative intensity – espe-cially the 671 cm^{-1} peak. The higher intensity in the 279 cm^{-1} band could underline a predominant formation of Na_2TiO_3 within the other titanate structures.

Fig. 9 shows the Raman spectra obtained on all the 295 V treated samples, where "A", "R" and "T" marks indicate anatase, rutile and sodium titanate, as above indicated. All four samples feature both "T" peaks: hence, if anodizing proceeds up to 295 V, Na ions from the electrolyte

Table 1
Fraction of anatase, calculated as the ratio between two anatase and rutile peaks – at 395 and 435 nm, respectively, or at 634 and 610 nm, respectively – as a function of the surface treatments: pre-etching, anodizing voltage and post-anodizing alkali etching.

Surface treatments (samples labels)			Anatase:rutile	
Etching	Voltage	Alkali etch	395:435	634:610
NE	175	–	0.60:0.40	0.57:0.43
NE	175	OH	0.70:0.30	0.66:0.34
E	175	–	0.60:0.40	0.55:0.45
E	175	OH	0.72:0.38	0.70:0.30
NE	295	–	0.74:0.36	0.66:0.34
NE	295	OH	0.57:0.63	0.69:0.31
E	295	–	0.54:0.66	0.42:0.58
E	295	OH	0.55:0.65	0.64:0.36

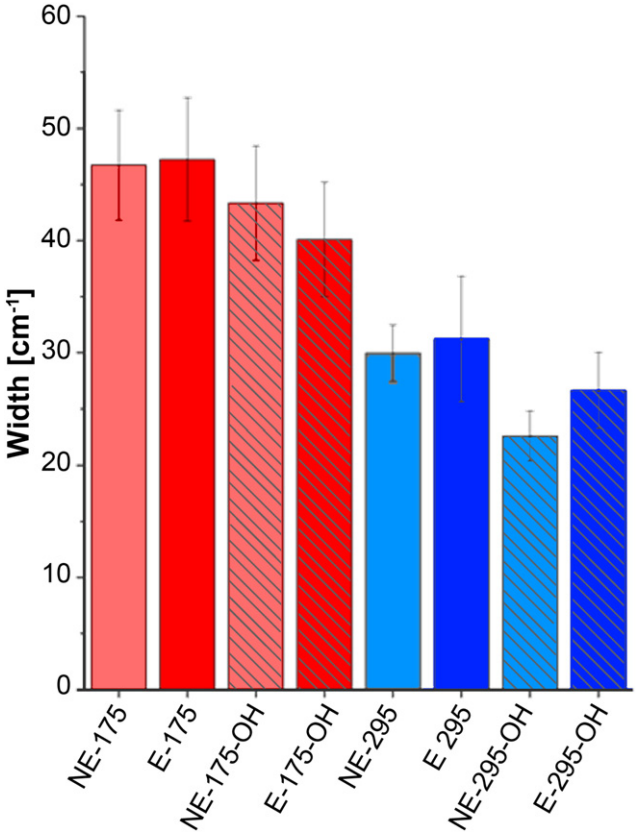

Fig. 10. Crystallinity of samples as calculated from full width at half maximum (FWHM) of anatase in Raman spectra at 513 cm^{-1}.

are directly incorporated in the TiO_2 lattice, with consequent formation of sodium titanate. In this case, the effect of the NaOH treatment is that of increasing the quantity of sodium titanates already present in the ma-terial. In fact, the relative intensity of "T" bands is higher than in ASD 175 V samples and reaches the maximum value on the NE 295 V + NaOH sample (Fig. 9c). The 671 cm^{-1} peak intensity and width, in particular, is higher than that of the NaOH post-treated 175 V samples, indicating the presence not only of Na_2TiO_3, but also of different sodium titanate stoichiometries.

Raman data demonstrate that the final alkali etching is associated not only with an increase in surface roughness, but also with the forma-tion of sodium titanates through the reaction of TiO_2 with NaOH and ex-pulsion of water, as proposed by Sun et al. [44]; Na^+ is incorporated in the TiO_2 lattice between the edge-shared [TiO_6] octahedral layers [44–46].

The deconvoluted anatase and rutile peaks intensities were used to estimate the effect of the treatment on the amount of phases present. As a general trend, it was observed that the anatase over rutile intensity ratio is usually higher in the 175 V samples when compared to the 295 V ASD ones. This effect can be due to a higher energy flux and larger crystallite dimension associated with the 295 V voltage which allowed the formation of higher amounts of rutile phase [47]. Nevertheless, the ratios are affected by a strong scattering and the relative intensities differed from point to point. More applied voltage steps are required in order to have a solid confirmation of a specific trend.

Fractions of anatase and rutile in the oxide were measured by applying a correlation between anatase and rutile peak intensities (anatase peak at 304 cm^{-1} vs rutile peak at 443 cm^{-1} the anatase peak at 636 cm^{-1} vs the rutile peak at 608 cm^{-1}) calibrated with mixtures of anatase and rutile with different ratios (see Appendix A). The results are summarized in Table 1. At 175 V, the amount of anatase increases from about 60% to about 70% after the NaOH post-treatment, while the pre-etching of the titanium substrate doesn't show a clear effect. In 295 V samples, the amount of anatase remains almost constant after the NaOH post-treatment and it is independent on the pre-etching.

The titanium oxide layers crystallinity was evaluated accounting the full width at half maximum (FWHM) of anatase Raman peak at 513 cm $^{-1}$; the peak at 395 cm^{-1} was also considered, but more scattered results were obtained – yet presenting similar trend (data not shown). The results are shown in Fig. 10. A lower FWHM was ob-served after anodizing at 295 V with respect to 175 V, which corre-sponds to a lower quantity of amorphous phase (higher crystallinity). In addition, the NaOH treatment has an effect on further enhancing an-atase crystallinity, probably preferentially dissolving the amorphous phase [48]. No significant differences could be observed between the etched and not-etched samples in absence of NaOH treatment.

Fig. 11 shows the peak intensity, position and FWHM of the sodium titanate peak at about 279 cm^{-1}. Peak intensity (Fig. 11a) is a function

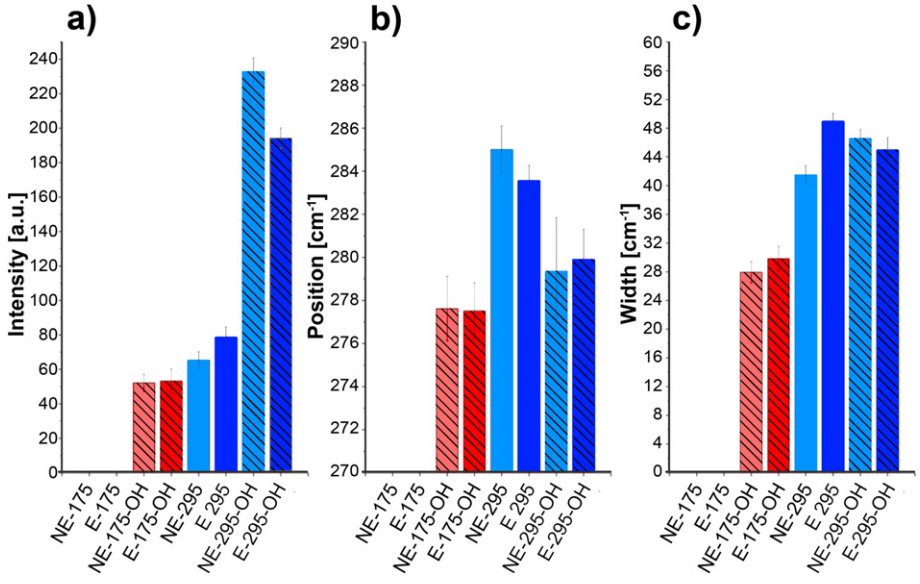

Fig. 11. a) peak intensity, b) position and c) FWHM of the sodium titanate peak at about 279 cm^{-1}.

of both ASD voltage and NaOH post-treatment. At the lower voltage, only the NaOH post-treatment is able to generate a sodium titanate phase, while anodizing at 295 V produces a higher titanate peak when compared with the 175 V + NaOH sample, meaning that high voltage anodizing is more effective in producing titanate phases than NaOH post-treatment. The combination of the two, anodizing and NaOH treat-ment, generates even larger quantities of titanates, with peaks almost three times more intense than those of the solely anodized sample. No significant effect of substrate etching on peak intensity could be ob-served at low voltage, while a slight effect – but not consistent in the dif-ferent treatments – was noticed at 295 V.

The peak position of the 175 V + NaOH (Fig. 11b), both with and without substrate etching, is close to the literature values for the Na_2TiO_3 phase, while peaks observed on the 295 V samples are wider and shifted to higher wavenumbers, associated to secondary sub-bands of additional sodium titanate $Na_xTi_yO_{xy\ +\ 1}$ stoichiometries. Hence, anodizing promotes the formation of different forms of titanates with respect to NaOH post-treatment, whose composition cannot be precisely differentiated in their exact stoichiometries on account of the only slight differences between possible titanates. The presence of at least two different sub-bands is also in line with the results obtained from the FWHM of the peak (Fig. 11c), where it can be observed that all the samples treated with the highest applied voltage feature a wider band.

4. Conclusions

In this work, the effects of HF etching, anodic spark deposition at dif-ferent applied voltages and alkali etching post treatment in NaOH on the surface morphology, crystal structure and chemical composition of the resulting titanium oxide layers were investigated.

The HF pre-treatment only affects surface roughness, with no signif-icant consequence on surface chemistry. Anodizing at 175 V and 295 V promoted the formation of a titanium oxide surface layer composed of anatase and rutile phases, but the higher voltage also triggered the for-mation of a mixture of sodium titanates with varying stoichiometries, while the NaOH post-treatment promoted the preferential formation of Na_2TiO_3 with respect to the other titanates. The combination of anod-izing and NaOH post-treatment has a synergetic effect on the produc-tion of sodium titanates.

The ability of the treatments to form sodium titanate and conse-quently increase the presence of radical species, which are likely to form in presence of a more disordered structure – intermixing of pure TiO_2 and titanates, and larger amount of defects and substoichiometry – are surely playing an important role in the interaction with the biological environment. Indeed, such peculiar surface features could explain the enhancement of bioactivity as well as the bacteriostatic effects of the treatments reported in previous biological studies.

Appendix A. Anatase/rutile quantification by Raman spectroscopy

A calibration was performed in order to evaluate the fraction amount of anatase and rutile in the different ASD layers using Raman spectroscopy. Commercially pure anatase (Wako, purity 98.5%) and rutile (Wako, purity 99.9%) powders were mixed at different concentrations (from 100% anatase to 100% rutile with 10% steps) and their Raman spectra were acquired. Results are shown in Fig. A1. With increasing amount of anatase in the mixture, the rutile related peaks become weaker and finally disappear, while the anatase related peaks gain intensity. Two couples of peaks were identified as potential candidates for the calibration, the anatase peak at 304 cm^{-1} vs the rutile peak at 443 cm^{-1} and the anatase peak at 636 cm^{-1} vs the rutile peak at 608 cm^{-1}. The two couples were then used in Fig. A2aandFig. A2bto evaluate the intensity ratio as a function of the anatase fraction. It can be observed that the trends of both ratios follow a rational function fashion, with an asymptote at x = 1. The coefficient is similar for both

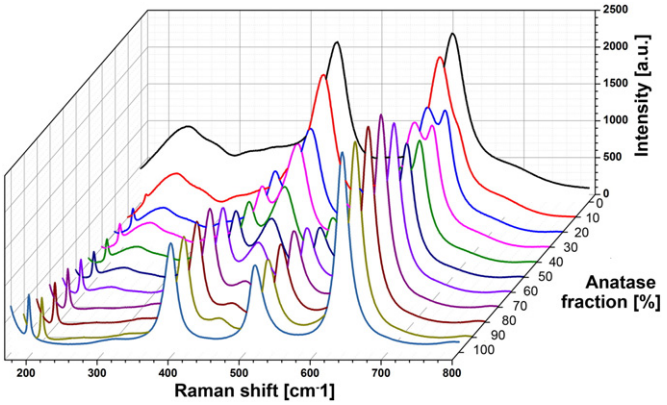

Fig. A1. Raman spectra of a mixture of anatase and rutile powders as a function of anatase percent fraction.

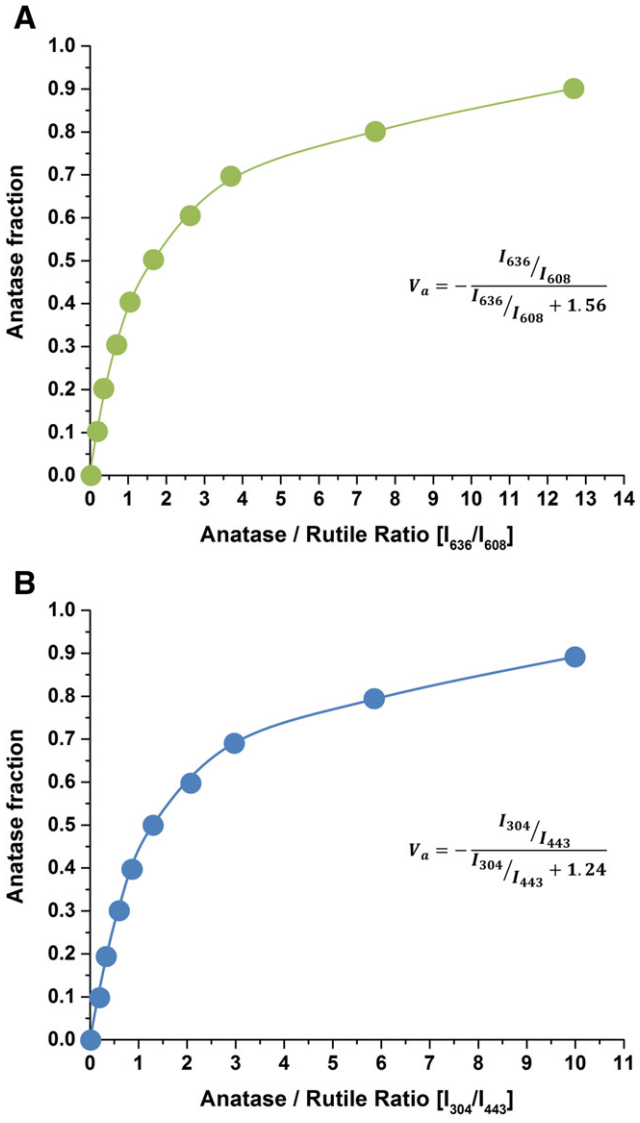

Fig. A2. Trend in the anatase to rutile peak intensity ratio as a function of anatase fraction, calculated on the basis of anatase peak at 636 cm^{-1} and rutile peak at 608 cm^{-1} (A) or of anatase peak at 304 cm^{-1} and rutile peak at 443 cm^{-1} (B).

numerators, 1.24 for I_{304}/I_{443} and 1.56 for I_{636}/I_{608} and both formulas have a R^2 determination higher than 99.99%.

References

[1] J.F. Vanhumbeeck, J. Proost, Current understanding of Ti anodization: functional, morphological, chemical and mechanical aspects, Corros. Rev. 27 (2009) 117–194.

[2] M.V. Diamanti, M.P. Pedeferri, M. Ormellese, Application-wise nanostructuring of anodic films on titanium: a review, J. Exp. Nanosci. 10 (2015) 1285–1308.

[3] Y. Oshida, Bioscience and Bioengineering of Titanium Materials: 2nd ed, Elsevier, Amsterdam, NL, 2012.

[4] M. Geetha, A.K. Singh, R. Asokamani, A.K. Gogia, Ti based biomaterials, the ultimate choice for orthopaedic implants - a review, Prog. Mater. Sci. 54 (2009) 397–425.

[5] Y. Wang, H. Yu, C. Chen, Z. Zhao, Review of the biocompatibility of micro-arc oxida-tion coated titanium alloys, Mater. Des. 85 (2015) 640–652.

[6] T.B. Van, S.D. Brown, G.P. Wirtz, Mechanism of anodic spark deposition, Am. Ceram. Soc. Bull. 56 (1977) 563–566.

[7] A. Krząkała, A. Kazek-Kęsik, W. Simka, Application of plasma electrolytic oxidation to bioactive surface formation on titanium and its alloys, RSC Adv. 3 (2013) 19725–19743.

[8] S.D. Brown, G.P. Wirtz, Formation of ceramic coatings by anodic spark deposition – a review, Proc. Electrochem. Soc. 86-11 (1986) 138–146.

[9] H. Dong, Tribological properties of titanium-based alloys, Surface Engineering of Light Alloys: Aluminium, Magnesium and Titanium Alloys, Woodhead Publishing Limited, Cambridge, UK 2010, pp. 58–80.

[10] J.J.T.M. Swartjes, P.K. Sharma, T.G. VanKooten, H.C. Van DerMei, M. Mahmoudi, H.J. Busscher, E.T.J. Rochford, Current developments in antimicrobial surface coatings for biomedical applications, Curr. Med. Chem. 22 (2015) 2116–2129.

[11] C. Della Valle, L. Visai, M. Santin, A. Cigada, D. Pezzoli, C.R. Arciola, M. Imbriani, R. Chiesa, A novel antibacterial modification treatment of titanium capable to improve osseointegration, Int. J. Artif. Organs 35 (2012) 864–875.

[12] A. Cochis, B. Azzimonti, C. Della Valle, R. Chiesa, C.R. Arciola, L. Rimondini, Biofilm formation on titanium implants counteracted by grafting gallium and silver ions, J. Biomed. Mater. Res. A 103A (2015) 1176–1187.

[13] H.A. Foster, I.B. Ditta, S. Varghese, A. Steele, Photocatalytic disinfection using titani-um dioxide: spectrum and mechanism of antimicrobial activity, Appl. Microbiol. Biotechnol. 90 (2011) 1847–1868.

[14] A.R. Khataee, M. Fatinia, Application of TiO_2 nanomaterials for photocatalytic de-struction of biological species and cancer therapy, in: M. Adeli (Ed.), Hybrid Nano-structures in Cancer Therapy, Nova Science Publisher, Hauppauge, N.Y. 2012, pp. 159–192.

[15] A. Markowska-Szczupak, K. Ulfig, A.W. Morawski, The application of titanium diox-ide for deactivation of bioparticulates: an overview, Catal. Today 169 (2011) 249–257.

[16] O. Carp, C.L. Huisman, A. Reller, Photoinduced reactivity of titanium dioxide, Progr. Solid State Chem. 32 (2004) 33–177.

[17] A. Fujishima, T.N. Rao, D.A. Tryk, Titanium dioxide photocatalysis, J. Photochem. Photobiol. C 1 (2000) 1–21.

[18] T.W. Ng, T. An, G. Li, W.G. Ho, H.Y. Yip, H. Zhao, P.K. Wong, The role and synergistic effect of the light irradiation and H_2O_2 in photocatalytic inactivation of *Escherichia coli*, J. Photochem. Photobiol. B 149 (2015) 164–171.

[19] A. Cochis, B. Azzimonti, C. Della Valle, E. De Giglio, N. Bloise, L. Visai, S. Cometa, L. Rimondini, R. Chiesa, The effect of silver or gallium doped titanium against the mul-tidrug resistant *Acinetobacter baumannii*, Biomaterials 80 (2016) 80–95.

[20] C.M. Sayes, R. Wahi, P.A. Kurian, Y. Liu, J.L. West, K.D. Ausman, D.B. Warheit, V.L. Colvin, Correlating nanoscale titania structure with toxicity: a cytotoxicity and in-flammatory response study with human dermal fibroblasts and human lung epithe-lial cells, Toxicol. Sci. 92 (2006) 174–185.

[21] A.M. Díez-Pascual, A.L. Díez-Vicente, Effect of TiO_2 nanoparticles on the performance of polyphenylsulfone biomaterial for orthopaedic implants, J. Mater. Chem. B 2 (2014) 7502–7514.

[22] J.H. Nicola, C.A. Brunharoto, M. Abramovich, C.E.T. Concalves da Silva, Second order Raman spectrum of rutile TiO_2, J. Raman Spectrosc. 8 (1979) 32–34.

[23] T. Ohsaka, F. Izumi, Y. Fujiki, Raman spectrum of anatase, TiO_2, J. Raman Spectrosc. 7 (1978) 321–324.

[24] V. Swamy, B.C. Muddle, Size-dependent modifications of the Raman spectrum of ru-tile TiO_2, Appl. Phys. Lett. 89 (2006) 163118.

[25] T. Ohsaka, S. Yamaoka, O. Shimomura, Effect of hydrostatic pressure on the Raman spectrum of anatase (TiO_2), Solid State Commun. 30 (1979) 345–347.

[26] I.A. Alhomoundi, G. Newaz, Residual stresses and Raman shift relation in anatase TiO_2 thin film, Thin Solid Films 517 (2009) 4372–4378.

[27] J. Wang, Q. Zhang, S. Yin, T. Sato, F. Saito, Raman spectroscopic analysis of sulphur-doped TiO_2 by co-grinding with TiS_2, J. Phys. Chem. Solids 68 (2007) 189–192.

[28] N. Mahdjoub, N. Allen, P. Kelly, V. Vishnyakov, SEM and Raman study of thermally treated TiO_2 anatase nanopowders: influence of calcination on photocatalytic activ-ity, J. Photochem. Photobiol. A 211 (2010) 59–64.

[29] M. Yuan, J. Zhang, S. Yan, G. Luo, Q. Xu, X. Wang, C. Li, Effect of Nd_2O_3 addition on the surface phase of TiO_2 and photocatalytic activity studied by UV Raman spectroscopy,
J. Alloys Compd. 509 (2011) 6227–6235.

[30] R. Li, A. Zhou, Q. Lu, C. Yang, J. Zhang, In situ monitoring and analysis of the photo-catalytic degradation process and machanism on recuclable Au NPs-TiO_2 NTs sub-strate using surface-enhanced Raman scattering, Colloid Surf. A 436 (2013) 270–278.

[31] X. Liu, N.J. Coville, A Raman study of titanate nanotubes, S. Afr. J. Chem. 58 (2005) 110–115.

[32] M. Takemoto, S. Fujibayashi, M. Neo, J. Suzuki, T. Matsushita, T. Kokubo, T. Nakamura, Osteoinductive porous titanium implants: effect of sodium removal by dilute HCl treatment, Biomaterials 27 (2006) 2682–2691.

[33] B.H. Lee, C. Lee, D.G. Kim, K. Choi, K.H. Lee, Effect of surface structure on biomechan-ical properties and osseointegration, Mater. Sci. Eng. C 28 (2008) 1448–1461.

[34] C. Della Valle, G. Rondelli, A. Cigada, A.E. Bianchi, R. Chiesa, A novel silicon-based electrochemical treatment to improve osteointegration of titanium implants, J. Appl. Biomater. Funct. Mater. 11 (2013) 106–116.

[35] M. Ocana, J.V. Garcia-Ramos, C.J. Serna, Low-temperature nucleation of rutile ob-served by Raman spectroscopy during crystallization of TiO_2, J. Am. Ceram. Soc. 75 (1992) 2010–2012.

[36] V. Swamy, Size-dependent modifications of the first-order Raman spectra of nano-structured rutile TiO_2, Phys. Rev. B 77 (2008) 195414.

[37] H. Liu, D. Yang, Z. Zheng, X. Ke, E. Waclawik, H. Zhu, R.L. Frost, A Raman spectroscop-ic and TEM study on the structural evolution of $Na_2Ti_3O_7$ during the transition to $Na_2Ti_6O_{13}$, J. Raman Spectrosc. 41 (2010) 1331–1337.

[38] T. Kokubo, S. Yamaguchi, Novel bioactive titanate layers formed on Ti metal and its alloys by chemical treatments, Materials 3 (2009) 48–63.

[39] T. Kokubo, S. Yamaguchi, Bioactive titanate layers formed on titanium and its alloys by simple chemical and heat treatments, Open Biomed. Eng. J. 9 (2015) 29–41.

[40] S.-H. Oh, R.R. Finõnes, C. Daraio, L.-H. Chen, S. Jin, Growth of nano-scale hydroxyap-atite using chemically treated titanium oxide nanotubes, Biomaterials 26 (2005) 4938–4943.

[41] H.-K. Ku, H.-J. Oh, K.-J. Noh, S.-C. Jung, K.-S. Park, W.-J. Lee, S.-J. Kim, Crystalline char-acterization and photodecomposition properties of rod-shaped $Na_2Ti_6O_{13}$ powder prepared by molten salt process, J. Nanosci. Nanotechnol. 11 (2011) 7269–7272.

[42] H. Liu, D. Yang, E.R. Waclawik, X. Ke, Z. Zheng, H. Zhu, R.L. Frost, A Raman spectro \-scopic study on the active site of sodium cations in the structure of $Na_2Ti_3O_7$ during the adsorption of Sr^{2+} and Ba^{2+} cations, J. Raman Spectrosc. 41 (2010) 1792–1796.

[43] D. He, P. Liu, X. Liu, F. Ma, X. Chen, W. Li, J. Du, P. Wang, J. Zhao, Characterization of hydroxyapatite coatings deposited by hydrothermal electrochemical method on NaOH immersed Ti6Al4V, J. Alloys Compd. 672 (2016) 336–343.

[44] X. Sun, X. Chen, Y. Li, Large-scale synthesis of sodium and potassium titanate nanobelts, Inorg. Chem. 41 (2002) 4996–4998.

[45] A. Nakahira, T. Kokubo, C. Numako, Formation mechanism of TiO_2-derived titanate nanotubes prepared by the hydrothermal process, Inorg. Chem. 49 (2010) 5845–5852.

[46] S.H. Lim, J. Luo, Z. Zhong, W. Ji, J. Lin, Room-temperature hydrogen uptake by TiO2 nanotubes, Inorg. Chem. 44 (2005) 4124–4126.

[47] M.V. Diamanti, M.P. Pedeferri, Effect of anodic oxidation parameters on the titanium oxides formation, Corros. Sci. 49 (2007) 939–948.

[48] J. Birch, T. Burleigh, Oxides formed on titanium by polishing, etching, anodizing, or thermal oxidizing, Corrosion 56 (2000) 1233–1241.